Nucleonic resonance excitations with linearly polarized photons in $\gamma p \to \omega p$

Qiang Zhao*
Institut de Physique Nucléaire, F-91406 Orsay Cedex, France
(Received 14 August 2000; published 5 January 2001)

In this work, an improved quark model approach to the ω meson photoproduction with an effective Lagrangian is presented. The *t*-channel *natural*-parity exchange is taken into account through the Pomeron exchange, while the *unnatural*-parity exchange is described by the π^0 exchange. With a very limited number of parameters, the available experimental data in the low energy regime can be consistently accounted for. We find that the beam polarization observables show sensitivities to some *s*-channel individual resonances in the $SU(6)\otimes O(3)$ quark model symmetry limit. Especially, the two resonances $P_{13}(1720)$ and $F_{15}(1680)$, which belong to the representation $[\mathbf{56}, {}^2\mathbf{8}, 2, 2, J]$, have dominant contributions over other excited states. Concerning the essential motivation of searching for ''missing resonances'' in meson photoproduction, this approach provides a feasible framework, on which systematic investigations can be done.

DOI: 10.1103/PhysRevC.63.025203 PACS number(s): 24.85.+p, 13.60.Le, 14.20.Gk, 12.39.−x

I. INTRODUCTION

The nonrelativistic constituent quark model (NRCQM) [1,2] predicts a much richer baryon spectroscopy than observed in $\pi N \to \pi N$ scatterings. This initiates the efforts of searching for those so-called ''missing resonances'' in other meson coupled channels, for example, ηN, $\Delta\pi$, $K\Lambda$, $K\Sigma$, ρN, ωN, ϕN, etc., to which those resonances might have stronger couplings and could be detected in experiment.

The availabilities of high-intensity electron and photon facilities from JLab, ELSA, ERSF, and SPring-8 provide accesses to exciting the nucleons with the clean electromagnetic probes. Abundant informations of the internal structures of nucleons and their excited states can be then derived in their consequent meson decays. Namely, the meson photoproduction via resonance excitations might be able to provide an ideal tool for the essential motivations [3–6]. It can be anticipated that in the near future, a large database for the study of baryon structures as well as their couplings to various meson channels can be established. Theoretical interests are also revived in this QCD subfield, which is nonperturbative in nature. Empirical or phenomenological prescriptions with QCD-inspired ingredients are therefore developed in history [7–11], which will be tested by the forthcoming data.

In this work, we will concentrate on the exclusive ω meson photoproduction, $\gamma p \to \omega p$. Exploring the available, but very limited, data in the literature [12–15], we aim at establishing a consistent framework for the study of the intermediate resonance excitations in this channel. Since large degrees of freedom will appear at the resonance region,[1] we adopt the quark model description of the baryon states for the nucleons and resonances in this reaction, which will significantly reduce the number of free parameters.

In Refs. [16,17], a quark model for the resonance excitations has been developed. Taking the advantages of the self-consistent quark model framework, the authors introduced an effective Lagrangian for the quark-vector-meson vertex, where the vector meson was treated as a pointlike elementary particle. At quark level, only two universal parameters for the vector and tensor couplings would appear in the resonance excitation terms.

However, that approach needs to be improved since the *t*-channel *natural*-parity exchange has not been taken into account there. Only the *unnatural*-parity π^0 exchange was included to describe the forward peaking phenomenon in $\gamma p \to \omega p$. Due to the absence of the *natural*-parity exchange, the interferences between the *unnatural*-parity exchange and the *s*- and *u*-channels might be overestimated in some polarization observables.

In this improved version, the *natural*-parity exchange will be included through a Pomeron exchange phenomenology. In our preliminary study [18], we have shown that the introduction of the *natural*-parity exchange can improve the description of the cross sections very significantly. Here, for the first time, a quantitative result is derived by following a parameter constraint scheme, although more rigorous constraints to the parameters are expected from the forthcoming data from GRAAL and JLab. The roles played by the *t*-channel *natural* and *unnatural*-parity exchanges are emphasized since a reliable estimation of this part should be the prerequisite for further study relevant to the nucleonic resonance excitations. One will see as follows, over a large energy region, the interferences between the *natural* and *unnatural*-parity exchanges provide good constraints to the *t*-channel processes, which makes it possible to highlight the roles played by the intermediate resonances. We also show that the *natural*-parity exchange is necessary to account for the missing cross sections when $E_\gamma > \sim 2.2$ GeV.

In Sec. II, an introduction of the quark-vector-meson coupling is presented in the $SU(6)\otimes O(3)$ quark model symmetry limit. Also, the *t*-channel Pomeron exchange model is summarized. In Sec. III, the numerical study of the resonance effects in the cross sections and beam polarization

*Present address: Dept. of Physics, Univ. of Surrey, Guildford, GU2 7XH, U.K. Electronic address: qiang.zhao@surrey.ac.uk

[1]In principle, for each resonance 24 numbers (12 independent amplitudes) are required to determine its transition matrix elements in vector meson photoproduction. In pseudoscalar meson photoproduction, eight numbers are required.

observables are presented. The conclusions and discussions are given in Sec. IV.

II. ω MESON PHOTOPRODUCTION AMPLITUDES

In this section, the three contributing processes in the ω meson photo-production are summarized.

A. *s*- and *u*-channel transition amplitudes

In the SU(6)$\otimes$O(3) symmetry limit, the quark-vector-meson coupling is described by the effective Lagrangian [16,17]:

$$L_{eff}=-\bar{\psi}\gamma_\mu p^\mu\psi+\bar{\psi}\gamma_\mu e_q A^\mu\psi + \bar{\psi}\left(a\gamma_\mu+\frac{ib\sigma_{\mu\nu}q^\nu}{2m_q}\right)\phi_m^\mu\psi, \quad (1)$$

where ψ and $\bar{\psi}$ represent the quark and antiquark field, respectively, and ϕ_m^μ denotes the vector meson field. The two parameters, a and b represent the vector and tensor couplings of the quark to the vector meson, respectively. m_q and e_q are the mass and charge of the constituent quark, respectively. For the quark model parameters, m_q and α (harmonic oscillator potential strength), the commonly used values 330 and 385 MeV are adopted, respectively. It should be noted that the values for α are different from that used in the previous study [17,18]. In this work, an overall investigation favors smaller values.

With such an effective coupling, the transition amplitudes for the *s*- and *u*-channel can be explicitly derived [17]. The intermediate resonances will be introduced in the harmonic oscillator basis. Resonances with masses less than 2 GeV are assigned to the states of $n\leqslant 2$ in the harmonic oscillator basis, and therefore can be taken into account explicitly in the NRCQM. Then, in the helicity space the amplitude for each resonance with spin J can be expressed as

$$H^J_{a\lambda_v}=\frac{2M_R}{s-M_R^2+iM_R\Gamma(q)}\sum_{\Lambda_f} d^J_{\Lambda_f,\Lambda_i}(\theta)A^V_{\Lambda_f}A^\gamma_{\Lambda_i}, \quad (2)$$

where s is the c.m. energy square and M_R is the resonance mass. $\Gamma(\mathbf{q})$ is the momentum dependence of the resonance width, which has been given in Ref. [17]. Λ_f and Λ_i are defined as $\Lambda_f\equiv\lambda_v-\lambda_2$, and $\Lambda_i\equiv\lambda-\lambda_1$. Here $\lambda_\gamma=\pm1$, $\lambda_v=0,\pm1$, $\lambda_1=\pm1/2$, and $\lambda_2=\pm1/2$ denote the helicities of the photon, ω meson, initial, and final state nucleon, respectively. $A^\gamma_{\Lambda_i}$ and $A^V_{\Lambda_f}$ are the helicity amplitudes for the photon excitation and vector meson decay of an intermediate resonance, respectively. $d^J_{\Lambda_f,\Lambda_i}(\theta)$ is the Wigner-d function which rotates the vector $A^\gamma_{\Lambda_i}$ from the initial state coordinate system to the final state coordinate system. States with $n>2$ are treated as degenerate.

In the case of the ω meson photoproduction, the *t*-channel and the seagull term from Eq. (1) vanish since they are proportional to the charge of the outgoing vector meson, and therefore vanish in the neutral vector meson productions. The nucleon pole terms have been explicitly included [17].

B. *t*-channel *natural* and *unnatural* parity exchange amplitudes

We use the Pomeron exchange model by Donnachie and Landshoff [19–22] to account for the *natural*-parity exchange. In such a model, the Pomeron mediates the long range interaction between a confined quark and a nucleon, and behaves rather like a $C=+1$ isoscalar photon. In Ref. [23], the formula for the ϕ meson photoproduction off proton has been derived. Based on the Regge phenomenology and the SU(3) flavor symmetry, the same picture can be applied to the ω and ρ meson photoproduction. Here, we summarize the main points as follows.

The Pomeron-nucleon coupling is described by the vertex

$$F_\mu(t)=3\beta_0\gamma_\mu F_1(t), \quad (3)$$

where β_0 is the coupling strength of the single Pomeron to a light constituent quark (u,d,s), and is the only adjustable parameter in this Pomeron exchange model. $F_1(t)$ is the isoscalar nucleon electromagnetic form factor, and has the following expression:

$$F_1(t)=\frac{(4M_N^2-2.8t)}{(4M_N^2-t)(1-t/0.7)^2}. \quad (4)$$

For the $\gamma\omega\mathcal{P}$ vertex ($\mathcal{P}$ denotes the Pomeron), the lowest order diagram for the quark pair creation in Ref. [22] is used for the $q\bar{q}$ creation, but has been extrapolated to the limit of $Q^2=0$, namely, the process with real photons. Meanwhile, a bare photon vertex is introduced for the quark-photon interaction, which has the same form as the quark-photon coupling in Eq. (1).

The ''on-shell approximation'' is adopted for the $q\bar{q}\omega$ vertex V_ν:

$$V_\nu\left(p-\frac{1}{2}q,p+\frac{1}{2}q\right)=f_\omega M_\omega\gamma_\nu, \quad (5)$$

where f_ω represents the coupling strength and is fixed by the ω radiative decay width $\Gamma_{\omega\to e^+e^-}=0.59$ keV [24] with the following relation:

$$\Gamma_{\omega\to e^+e^-}=\frac{8\pi\alpha_e^2\hat{e}_q^2}{3}\left(\frac{f_\omega^2}{M_\omega}\right), \quad (6)$$

where $\hat{e}_q$ is the charge factor of quark q in terms of the charge of electron.

Therefore the current matrix element can be written as

$$\langle p_f m_f,q\lambda_v|J^\mu|p_i m_i\rangle = 2\beta_0 t^{\mu\alpha\nu}(k,q)\varepsilon_{m\nu}(q)\mathcal{G}_\mathcal{P}(s,t)\bar{u}(p_f)F_\alpha(t)u(p_i), \quad (7)$$

where $u(p_i)$ and $\bar{u}(p_f)$ are the initial and final state Dirac spinors of the protons with four-momenta p_i and p_f, respectively. k and q are the four momenta of the incoming photon

and outgoing ω meson, respectively. $\varepsilon_{m\nu}$ is the polarization vector of the produced ω meson, and the factor 2 counts the equivalent contributions from Pomeron-quark and Pomeron-antiquark interactions. $\mathcal{G}_{\mathcal{P}}(s,t)$ is related to the Regge trajectory of the Pomeron and has the form

$$\mathcal{G}_P(s,t) = -i(\alpha' s)^{\alpha(t)-1}, \tag{8}$$

where $\alpha(t)=1+\epsilon+\alpha' t$ is the Regge trajectory of the Pomeron. The form factor $\mu_0^2/(\mu_0^2+p^2)$ is introduced for each off-shell quark line with four-momentum p. The same parameter values as used in Ref. [22] are adopted: $\epsilon=0.08$, $\alpha'=0.25\ \mathrm{GeV}^{-2}$, $\mu_0=1.2$ GeV.

In Eq. (7), $t^{\mu\alpha\nu}(k,q)$ represents the loop tensor and it has the following expression for the contributing terms:

$$t^{\mu\alpha\nu}(k,q) = (k+q)^{\alpha} g^{\mu\nu} - 2k^{\nu} g^{\alpha\mu}. \tag{9}$$

To preserve gauge invariance, we have adopted the transformation given in Ref. [25].

In Ref. [23], we have shown that the polarization observables at large angles depend more on the spin structures of the *s*- and *u*-channel transition amplitudes rather than on the Pomeron exchange amplitude structure even the Pomeron exchange plays dominant role there. This feature suggests that the Pomeron phenomenology does not influence the large angle behaviors significantly. Otherwise, the large angle behaviors might be ''distorted'' in the polarization observables.

The formulas for the π^0 exchange terms in the ω meson photoproduction have been derived in Ref. [17]. Since the πNN and $\omega\pi\gamma$ couplings are quite well known, the only parameters left is the form factor from the quark model, which is to describe the combined effects from the two nonperturbative vertices. Taking into account the diffractive Pomeron exchange contribution, we have to adopt a smaller value $\alpha_\pi=290$ MeV for the form factor $e^{-(\mathbf{q}-\mathbf{k})^2/6\alpha_\pi^2}$. The determination of α_π will be discussed later.

III. NUMERICAL RESULTS

In this section, the unpolarized differential cross sections, density matrix elements of the vector meson, and beam polarization observables in the ω meson photoproduction are investigated. In $\gamma p \to \omega p$, the isospin conservation eliminates contributions from intermediate states with isospin 3/2. In addition, the Moorhouse selection rules [26] eliminate those nucleonic states of representation $[\mathbf{70}, {}^{4}\mathbf{8}, n, L, J]$ in the NRCQM from contributing. Therefore only eight intermediate nucleonic resonances contribute for $n \leqslant 2$ in the harmonic oscillator basis, i.e., $P_{11}(1440)$, $S_{11}(1535)$, $D_{13}(1520)$, $P_{13}(1720)$, $F_{15}(1680)$, $P_{11}(1710)$, $P_{13}(1900)$, $F_{15}(2000)$ [24]. In the notation for the quark model representation, the first three bold digitals denote the dimensions of the SU(6) (spin-flavor), SU(2) (spin), and SU(3) (flavor) groups, respectively. n, L, and J denote the main quantum number, total orbital angular momentum, and total spin of a three-quark baryon system in the harmonic oscillator basis. In this convention, one can express, for example, the proton and neutron ground state as $[\mathbf{56}, {}^{2}\mathbf{8}, 0, 0, 1/2]$.

Notice that Y. Oh *et al.* recently studied the resonance excitations in the ω meson photo-production [27]. In their approach, the N^* resonances are introduced by employing the quark model predictions [9,10] on the resonance photo-excitations and their decays into ωN. Therefore only those resonances with masses above the ωN threshold can be taken into account. In our model, the low-lying resonances, for example, $S_{11}(1535)$ and $D_{13}(1520)$, are found still have considerable contributions, which can be seen in the beam polarization asymmetries. We expect that forthcoming data should be helpful to clarify the roles played by those below-threshold resonances.

Before proceeding to the details of the numerical calculations, we summarize the scheme of determining the parameters as follows.

Since it has been well established that the high-energy ω production is dominated by the diffractive *natural*-parity exchange, we take the advantages of high energy measurements for the ω meson photoproduction by applying this Pomeron exchange model to ~ 10 GeV, where other processes become negligible. Then, the parameter $\beta_0=1.27$ can be derived. In fact, this parameter is the same as used in Ref. [23], which shows that the SU(3) flavor symmetry has been conserved for the light quark sector.

Above the resonance region ($E_\gamma \geqslant 2.2$ GeV), the interferences between the *t*-channel *natural* and *unnatural*-parity exchanges can be seen at forward angles up to ~ 5 GeV [14], where the *s*- and *u*-channel contributions are negligible. It provides an important constraint to the π^0 exchange terms. Therefore the parameter $\alpha_\pi=290$ MeV can be determined.

Concerning the two parameters introduced for the *s* and *u* channels, we require that a flattened behavior appearing at large angles for the differential cross section as shown by the old data [13], as well as the preliminary data from SAPHIR [12] and CLAS [28]. Meanwhile, the total cross sections [13–15] can provide constraints to the magnitudes of the parameters. Here, we find that with $a=-2.5$, and $b=-6.5$, a flattened structure is produced at large angles, and the energy evolutions of the cross sections can be reasonably reproduced.[2]

It should be pointed out that in this scheme the roles played by the *t*-channel processes and the *s* and *u* channel have been highlighted. We stress this feature since it is the prerequisite for the motivation of studying resonance phenomena when other processes are present. Although the final determination of the two parameters *a* and *b* needs more constraints from experiment, it can still provide us with quantitative informations related to the nucleonic resonance excitations, especially in the polarization observables.

A. Cross sections

Using the parameters determined through the above scheme, our first step is to study the cross section.

[2]In Ref. [18], the values for parameters *a* and *b* have been presented by inappropriately multiplying $(2L+1)$ for each resonance with total angular momentum L. *a* and *b* lost their original meanings. This problem has been corrected here.

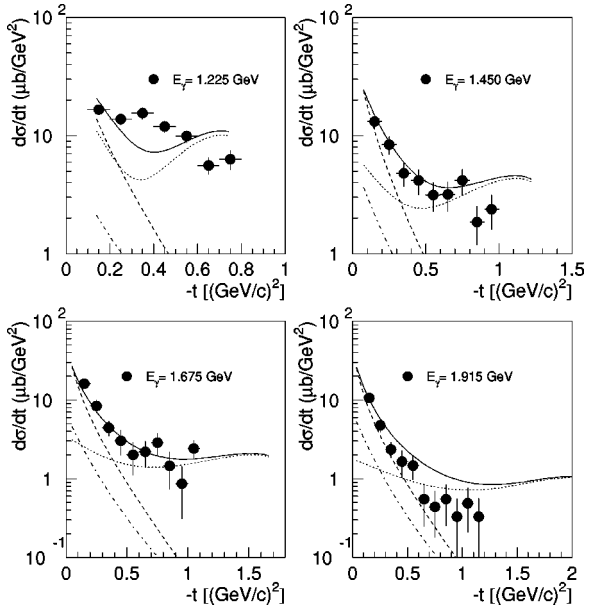

FIG. 1. Differential cross sections for $\gamma p \to \omega p$. The solid curves denote the full calculations, while the dashed, dotted, and dot-dashed curves denote the exclusive calculations of the π^0 exchange, *s*- and *u*-channels, and Pomeron exchange, respectively. The data are from the SAPHIR Collaboration [12].

In Fig. 1, we restudied the differential cross sections at four energy scales, $E_\gamma = 1.225$, 1.45, 1.675, and 1.915 GeV. As a comparison, the exclusive contributions from the three channels are also presented. At forward angles, the pion exchange (dashed curves) accounts for the steep forward peakings. The Pomeron exchange (dot-dashed curves) has quite small contributions at this energy region. However, we can see below, this small part will play important roles in some polarization observables.

Notice that near threshold, the *s*- and *u*-channel contributions (dotted curves) dominate over the *t*-channel π^0 exchange. This character can be justified by the precise measurements of the angular distributions. Nevertheless, the polarization observables should be able to provide more rich information relevant to the the resonance interferences.

The multiplets of representation $[\mathbf{56}, {}^2\mathbf{8}, 2, 2, J]$ in the quark model are found dominating over the other low-lying states in the cross sections. In the quark model, the resonances $P_{13}(1720)$ and $F_{15}(1680)$ are attributed to the $[\mathbf{56}, {}^2\mathbf{8}, 2, 2, J]$ representation with $J = 3/2$ and 5/2, respectively, in the harmonic oscillator basis, while the $P_{13}(1900)$ and $F_{15}(2000)$, to the $[\mathbf{70}, {}^2\mathbf{8}, 2, 2, J]$ representation. With the same couplings of the constituent quark to the ω meson as other intermediate states, the contributions from the resonances $P_{13}(1720)$ and $F_{15}(1680)$ are found much larger than that from resonances $P_{13}(1900)$ and $F_{15}(2000)$. Comparing the two representations $[\mathbf{56}, {}^2\mathbf{8}, 2, 2, J]$ and $[\mathbf{70}, {}^2\mathbf{8}, 2, 2, J]$ we find that two main features in their excitations lead to such a large difference. The first feature is that the configuration of $[\mathbf{56}, {}^2\mathbf{8}, 2, 2, J]$ permits its transitions to the nucleon ground state via the spin and orbital angular momentum splitting or nonsplitting terms. Therefore the three independent meson transition amplitudes $A^V_{1/2}$, $A^V_{3/2}$, and $S^V_{1/2}$ are all contributing.

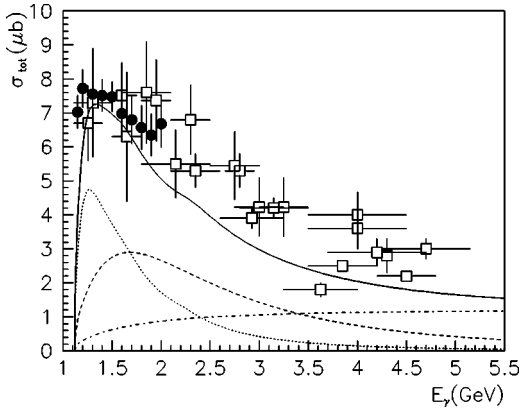

FIG. 2. Total cross sections for $\gamma p \to \omega p$. Notations are the same as Fig. 1. Data come from Ref. [12] (full dot) and Refs. [13–15] (empty square).

However, for the transitions of the $[\mathbf{70}, {}^2\mathbf{8}, 2, 2, J]$ to the nucleon ground state, the only nonvanishing amplitude is the $A^V_{1/2}$ due to the spin-splitting operator [17]. This feature suggests that states of $[\mathbf{56}, {}^2\mathbf{8}, 2, 2, J]$ have larger transition space to ωN than those of $[\mathbf{70}, {}^2\mathbf{8}, 2, 2, J]$. The second feature comes from the mass differences between these two sets of resonances. The $P_{13}(1720)$ and $F_{15}(1680)$ have the masses close to the ω production threshold, thus they have larger absorption amplitudes than the $P_{13}(1900)$ and $F_{15}(2000)$ near threshold. The dominant $P_{13}(1720)$ and $F_{15}(1680)$ can be seen significantly in the beam polarization observables.

In Fig. 2, the total cross sections for the three different processes are explicitly illustrated. Near threshold, the *s*- and *u*-channel contributions dominate over the *t*-channel π^0 exchange. As shown in the angular distributions, the cross section is dominated by the large angle mechanisms which are essentially governed by the resonance excitations. However, this contribution falls down quickly with the increasing energy. Above $E_\gamma = 3$ GeV, the *t*-channel processes become dominant, especially at the forward angles. The energy evolution of the cross sections indicates the change of the relative strengths for these three mechanisms. As shown by the dashed and dot-dashed curves, above 3 GeV the interferences between the Pomeron and π^0 exchanges will determine the forward angle behaviors for most observables. This feature provides us the opportunity of fixing the parameters of the *t*-channels.

With the Pomeron exchange contribution, the model improves the calculations when the energy goes above $E_\gamma \sim 2.2$ GeV [17,29].

B. Density matrix elements and parity asymmtry observables

In vector meson photoproduction, the final state vector meson decays ($\omega \to \pi^+ \pi^- \pi^0$) provide access to the measurements of the vector meson decay density matrix elements, which can be related to the vector or tensor polarizations of the vector meson, or angular distributions of the cross sections [30]:

$$W(\cos\theta,\phi,\Phi)=W^0(\cos\theta,\phi,\rho^0_{\alpha\beta})-P_\gamma\cos 2\Phi W^1(\cos\theta,\phi,\rho^1_{\alpha\beta})-P_\gamma\sin 2\Phi W^2(\cos\theta,\phi,\rho^2_{\alpha\beta})+\lambda_\gamma P_\gamma W^3(\cos\theta,\phi,\rho^3_{\alpha\beta}),\quad(10)$$

where

$$W^0(\cos\theta,\phi,\rho^0_{\alpha\beta})=\frac{3}{4\pi}\left(\frac{1}{2}\sin^2\theta+\frac{1}{2}(3\cos^2\theta-1)\rho^0_{00}-\sqrt{2}\,\mathrm{Re}\,\rho^0_{10}\sin 2\theta\cos\phi-\rho^0_{1-1}\sin^2\theta\cos 2\phi\right),\quad(11)$$

$$W^1(\cos\theta,\phi,\rho^1_{\alpha\beta})=\frac{3}{4\pi}(\rho^1_{11}\sin^2\theta+\rho^1_{00}\cos^2\theta-\sqrt{2}\,\mathrm{Re}\,\rho^1_{10}\sin 2\theta\cos\phi-\rho^1_{1-1}\sin^2\theta\cos 2\phi),\quad(12)$$

$$W^2(\cos\theta,\phi,\rho^2_{\alpha\beta})=\frac{3}{4\pi}(\sqrt{2}\,\mathrm{Im}\,\rho^2_{10}\sin 2\theta\sin\phi+\mathrm{Im}\,\rho^2_{1-1}\sin^2\theta\cos 2\phi),\quad(13)$$

$$W^3(\cos\theta,\phi,\rho^3_{\alpha\beta})=\frac{3}{4\pi}(\sqrt{2}\,\mathrm{Re}\,\rho^3_{10}\sin 2\theta\sin\phi+\mathrm{Im}\,\rho^3_{1-1}\sin^2\theta\sin 2\phi).\quad(14)$$

In the above equations, θ and ϕ are the polar and azimuthal angles of the normal direction of the ω decay plane with respect to the z axis in the production plane, which in the helicity frame is defined as the direction of the ω meson momentum. Φ is the angle of the photon polarization vector with respect to the production plane.

In the helicity space, the density matrix elements can be explicitly expressed in terms of the 12 independent helicity amplitudes:

$$\rho^0_{ik}=\frac{1}{A}\sum_{\lambda\lambda_2\lambda_1}H_{\lambda_{v_i}\lambda_2\lambda\lambda_1}H^*_{\lambda_{v_k}\lambda_2,\lambda\lambda_1},$$

$$\rho^1_{ik}=\frac{1}{A}\sum_{\lambda\lambda_2\lambda_1}H_{\lambda_{v_i}\lambda_2,-\lambda\lambda_1}H^*_{\lambda_{v_k}\lambda_2,\lambda\lambda_1},$$

$$\rho^2_{ik}=\frac{i}{A}\sum_{\lambda\lambda_2\lambda_1}\lambda H_{\lambda_{v_i}\lambda_2,-\lambda\lambda_1}H^*_{\lambda_{v_k}\lambda_2,\lambda\lambda_1},$$

$$\rho^3_{ik}=\frac{i}{A}\sum_{\lambda\lambda_2\lambda_1}\lambda H_{\lambda_{v_i}\lambda_2,\lambda\lambda_1}H^*_{\lambda_{v_k}\lambda_2,\lambda\lambda_1},\quad(15)$$

and

$$A=\sum_{\lambda_{v_i}\lambda\lambda_2\lambda_1}H_{\lambda_{v_i}\lambda_2,\lambda\lambda_1}H^*_{\lambda_{v_i}\lambda_2,\lambda\lambda_1},\quad(16)$$

where ρ_{ik} stands for $\rho_{\lambda_{v_i}\lambda_{v_k}}$, and $\lambda_{v_i},\lambda_{v_k}$ denote the helicity of the produced vector mesons. A is the cross section function. With the linearly polarized photon beam, ρ^0_{ik}, ρ^1_{ik}, and ρ^2_{ik} can be measured while with the circularly polarized photon beam, ρ^0_{ik} and ρ^3_{ik} can be measured. With the additional relations, $\rho^0_{00}+2\rho^0_{11}\equiv 1$, which represents the normalized cross section, only 11 elements are linearly independent.

At high energies, the experimental data for vector meson photoproduction exhibit characters of *t*-channel *natural*-parity exchange dominance and *s*-channel helicity conservation (SCHC). From high energy down to the resonance region, deviations from these features are expected due to the resonance excitations and the *t*-channel *unnatural*-parity exchange. Such an interference due to the different relative strength and mechanisms can be illustrated by the density matrix elements. Concerning the *t*-channel *natural* and *unnatural*-parity exchanges, some model-independent features can be learned [30]:

(i) Supposing only the *natural*-parity Pomeron exchange contributes in the diffractive phenomena, it can be justified that except that ρ^0_{11}, ρ^1_{1-1}, and $\mathrm{Im}\,\rho^2_{1-1}$ have a value of 0.5, other density matrix elements vanish.

(ii) For the exclusive *unnatural*-parity exchange, one has $\rho^0_{11}=0.5$, $\rho^1_{1-1}=-0.5$, and $\mathrm{Im}\,\rho^2_{1-1}=-0.5$, while the other elements will vanish.

(iii) In the π^0 exchange terms, the spin operator does not flip the helicity of the photon, therefore, the transition $\lambda_\gamma=\pm 1$ to $\lambda_v=0$ vanish.

In the model for the Pomeron exchange, although the Pomeron behaves rather like a $C=+1$ isoscalar photon, those spin splitting terms will be significantly suppressed in the forward angles [23], therefore the transition $\lambda_\gamma=\pm 1$ to $\lambda_v=0$ ''vanishes'' in the forward angles, which makes this process like a 0^{++} quantum number exchange process. Consequently, the element ρ^0_{00} vanishes in the forward direction due to the dominant *natural* or *unnatural*-parity exchanges in the small momentum transfer.

In Figs. 3–5, the density matrix elements ρ^0_{ik}, ρ^1_{ik}, and ρ^2_{ik} involved in the measurement of Ref. [14] are studied at small t regions for $E_\gamma=2.8$, 4.7, and 9.3 GeV from left to right in each row. It should be pointed out that the nonrelativistic resonance excitation model might meet trouble when applied to high energies, for example, $E_\gamma>3$ GeV. However, notice that this process decreases exponentially with the increasing energy, and becomes negligible around 3 GeV; our study of the constraints to the *t*-channel processes do not suffer troubles arising from this shortcoming, especially at forward angles.

In Figs. 3–5, the solid curves present the exclusive calculations for the *t*-channel reactions. The full calculations are illustrated through the dashed curves. It shows that at $E_\gamma=2.8$ GeV, the resonance excitations have become negligible for most of the elements. For $E_\gamma=9.3$ GeV, the dashed curves cannot be distinguished from the solid ones. Here,

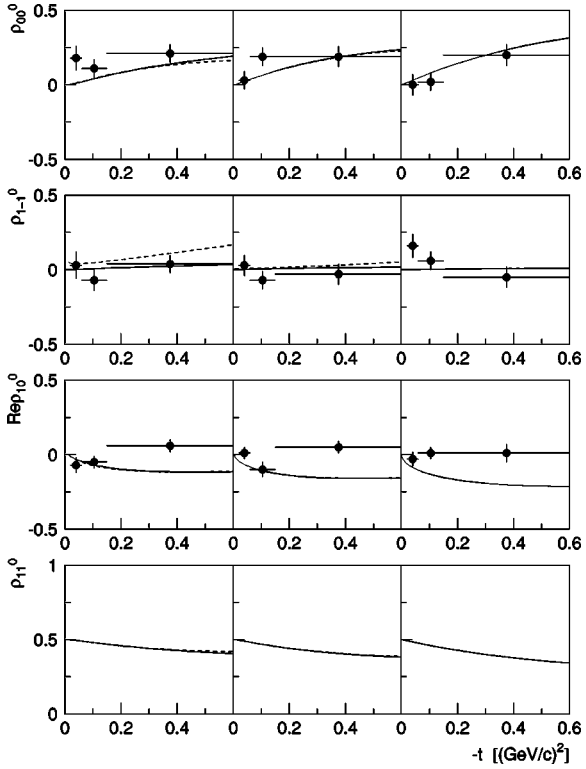

FIG. 3. Density matrix elements ρ_{ik}^0. From left to right for each row, the photon energy E_γ will be 2.8, 4.7, and 9.3 GeV, respectively. The solid curves denote the calculations of the *t*-channel π^0 and Pomeron exchange. The dashed curves denote the full calculations. Data are from [14].

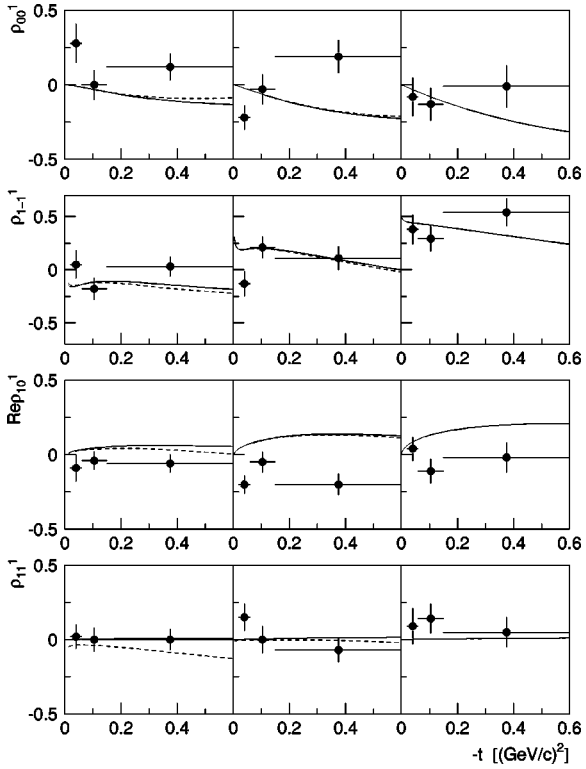

FIG. 4. Density matrix elements ρ_{ik}^1. The notations are the same as Fig. 3.

although the data [14] for the density matrix elements are very sparse, they provide an interesting test of the model of *t*-channel π^0 and Pomeron exchanges, which will essentially determine the forward angle behaviors of the density matrix elements.

As summarized in former paragraph, the nonzero elements ρ_{11}^0, ρ_{1-1}^1, and $\mathrm{Im}\,\rho_{1-1}^2$ will reflect the interferences between these two processes. In Fig. 3, the calculations of the elements ρ_{00}^0, ρ_{1-1}^0, and $\mathrm{Re}\,\rho_{10}^0$ are in good agreement with the data for small *t*. There is no datum available for the ρ_{11}^0 in experiment. An interesting feature for this element is that it will have the value 0.5 at forward angles for both *natural* and *unnatural*-parity exchanges. The close-to-0.5 value we find might suggest that this element does not involve strong interferences within these two *t*-channel processes.

Comparing the ρ_{1-1}^1 at these three energies in Fig. 4, one can see that the data have been reproduced impressively. The relative strengths between the π^0 and Pomeron exchanges as well as the energy evolutions for these two terms are essential for reproducing this element. At 2.8 GeV, the *unnatural*-parity exchange dominates over the *natural*-parity one, and thus produces negative values for this element. With the increasing energy, the *natural*-parity exchange becomes dominant. Therefore, at 4.7 GeV, positive values for the ρ_{1-1}^1 are found. At 9.3 GeV, the value reaches 0.5, which suggests that the Pomeron exchange has absolutely dominated over other processes.

For most of the elements, our calculations are in good agreement with the measurement except for the $\mathrm{Im}\,\rho_{1-1}^2$ at 9.3 GeV in Fig. 5, where large discrepancies are found. Interestingly, as summarized at the beginning of this section, at 9.3 GeV, the *natural*-parity exchange becomes dominant, therefore it will have the value 0.5 at forward angles. The calculation consistently output this feature, while, however, the measurement provides small negative values. The data here cannot be explained by the influences from the *unnatural*-parity exchange and the *s*- and *u*-channel resonance excitations due to their small cross section at this energy region. A precise measurement for this element should be important to clarify the discrepancies.

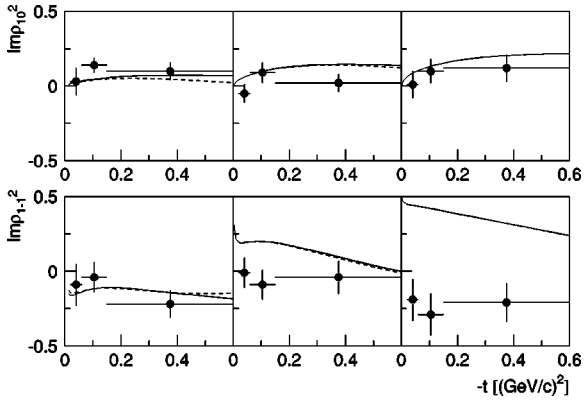

FIG. 5. Density matrix elements ρ_{ik}^2. The notations are the same as Fig. 3.

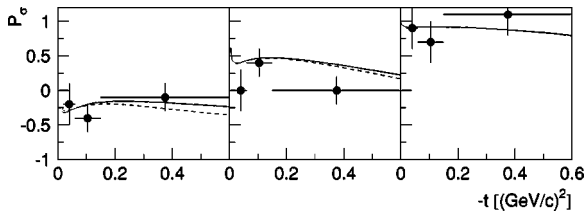

FIG. 6. Parity asymmetry P_σ. The notations are the same as Fig. 3.

Concerning the mechanism of the *t*-channel parity exchanges, one can investigate the parity asymmetry observable P_σ, which can be related to two of the density matrix elements, ρ^1_{1-1} and ρ^1_{00}:

$$P_\sigma = 2\rho^1_{1-1} - \rho^1_{00}. \tag{17}$$

These two elements can be determined in the linearly polarized photon beam measurement. As discussed above, in the pure *natural*-parity exchange process, $\rho^1_{1-1}=0.5$ and $\rho^1_{00}=0$ will result in $P_\sigma=+1$. Similarly, if the *unnatural*-parity exchange process contributes exclusively, one will get $P_\sigma=-1$ with $\rho^1_{1-1}=-0.5$ and $\rho^1_{00}=0$. At high energies and at the forward angles, the deviation of the parity asymmetries from $+1$ or -1 will suggest that both *natural* and *unnatural*-parity exchanges exist in the reaction. However, such a conclusion cannot be applied to the low energy region due to the presence of resonance excitations, which will violate the *s*-channel helicity conservation, and shift the parity asymmetry away from $+1$ or -1. In other words, if one expects to disentangle information relevant to the resonance excitations, the prerequisite is to consistently include the *natural*-parity exchange interference.

The results for P_σ at $E_\gamma=2.8$, 4.7, and 9.3 GeV are shown in Fig. 6. It shows that at 2.8 GeV, the *unnatural*-parity π^0 exchange is dominant, thus negative asymmetries are produced. With the increasing energy, the *natural*-parity Pomeron exchange becomes more and more important and then the asymmetry will change to positive. At 9.3 GeV, the π^0 and resonance excitations become negligible and the dominant Pomeron exchange produces the parity asymmetries very close to $+1$. Apparently, the parity asymmetry at high energies and forwards angles shows great sensitivities to the underway *natural* or *unnatural*-parity exchange mechanisms.

The dashed curves illustrate the effects if the *s*- and *u*-channel resonance excitations are taken into account. One can see that their effects at small *t* is quite negligible. It confirms the scheme to determine the *t*-channel parameters at higher energies, and then apply them to the resonance region.

C. Beam polarization observables

The polarization observable asymmetries become interesting since contributions from individual resonances might be amplified in the polarization observables, and therefore produce a detectable effect. In comparison with the density matrix elements, here one selects the experimental situation by polarizing the spin of the initial and/or final state particles.

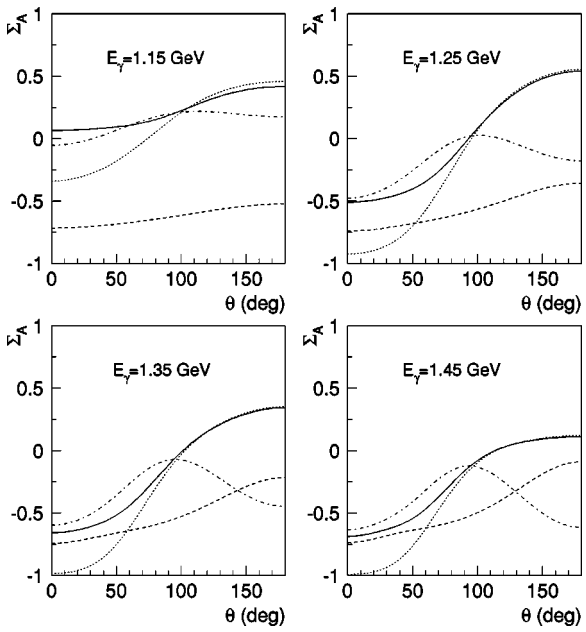

FIG. 7. Beam polarization asymmetry $\check{\Sigma}_A$ at four energy scales. The solid curves denote the full calculations, while the dashed curves denote results of the *t*-channel π^0 and Pomeron exchange, and the dotted curves, of π^0 plus *s*- and *u*-channels. The dot-dashed curves denote the $P_{13}(1720)$-absent effects in the full calculations.

In particular, with the linearly polarized photon beam, the first three terms in Eq. (10) can be measured. In the final state ω meson decay plane, one can select $\Phi=0°$, thus the third term in Eq. (10) vanishes and only W^0 and W^1 have contributions. At the direction $\phi=90°$ and $\theta=90°$, one obtains

$$W(\cos 90°, 90°, 0°) = \frac{3}{4\pi}\left[\frac{1}{2} - \frac{1}{2}\rho^0_{00} + \rho^0_{1-1}\right] - P_\gamma \frac{3}{4\pi}[\rho^1_{11} + \rho^1_{1-1}]. \tag{18}$$

With the relation $2\rho^0_{11}+\rho^0_{00}=1$, the beam polarization asymmetry is defined as

$$\check{\Sigma}_A \equiv \frac{\rho^1_{11}+\rho^1_{1-1}}{\rho^0_{11}+\rho^0_{1-1}} = \frac{\sigma_\parallel - \sigma_\perp}{\sigma_\parallel + \sigma_\perp}, \tag{19}$$

where $\sigma_\parallel$ represents the pion cross section of the ω meson decay with the pions submerged in the photon polarization plane, while $\sigma_\perp$ represents that with the pions perpendicular to it.

In Fig. 7, $\check{\Sigma}_A$ is investigated for four energy scales, i.e., $E_\gamma=1.15$, 1.25, 1.35, and 1.45 GeV within the energy access of the GRAAL Collaboration. The solid curves denote the full calculations, while the dashed curves denote the exclu-

sive calculations with the *t*-channel processes. The dotted curves are obtained by eliminating the Pomeron exchange in the full calculations.

Note that, for the pure *natural*-parity exchange process, one has $\check{\Sigma}_A=+1$, while for the pure *unnatural*-parity exchange, $\check{\Sigma}_A=-1$.[3]

Here, several lessons can be learned:

(A) As shown by the dashed curves, the negative asymmetries are due to the dominant π^0 exchange at low energy regions.

(B) Comparing the dashed curves to the solid ones, one can see that the influences from the *s*- and *u*-channels are very significant, especially near threshold.

(C) The effects from the *natural*-parity exchange are shown explicitly at forward angles by the dotted curves. This process has very small cross sections at low energies, and therefore cannot be seen clearly in the angular distributions. However, it intervenes strongly at forward angles in $\check{\Sigma}_A$ and deviates the asymmetries from -1. This feature confirms our argument that a reliable description of the *t*-channel processes should be important in the study of the polarization observables concerning the resonance excitations.

(D) The large angle asymmetries are dominated by the *s*- and *u*-channel processes, in which signals for some individual resonances can be derived.

In the ω meson production, the most interesting resonance should be the $P_{13}(1720)$, of which the coupling to the ωN channel has not been established in experiment. As summarized in the previous subsection, the relatively large contributions from the $P_{13}(1720)$ are due to its NRCQM configuration and near-threshold mass.

However, according to the PDG [24], the $P_{13}(1720)$ couples more strongly to the isovector ρ than to the isoscalar ω meson. A question arising here should be whether one can find signals for the presence of the $P_{13}(1720)$ given the beam polarization data available.

In this calculation, we find that the beam polarization asymmetries are also very sensitive to the $P_{13}(1720)$ excitation. Supposing the $P_{13}(1720)$ has no coupling to the ωN channel, we present the $P_{13}(1720)$-absent asymmetries with the dot-dashed curves in Fig. 7. Very significant effects are found at backward angles, while the influences at forward angles are found negligible. Such an effect can be tested by the measurements of GRAAL and CLAS.

With $\phi=0°$, $\theta=90°$, and $\Phi=0°$ in Eq. (10), one can define another observable:

$$\check{\Sigma}_B=\frac{\rho^1_{11}-\rho^1_{1-1}}{\rho^0_{11}-\rho^0_{1-1}}. \tag{20}$$

It can be easily seen that for the exclusive *natural* or *unnatural*-parity exchanges, $\check{\Sigma}_B$ has values -1 or $+1$, respectively, which are opposite to the cases for $\check{\Sigma}_A$. When both processes exist in the reaction, a deviation from $+1$ or -1 is expected.

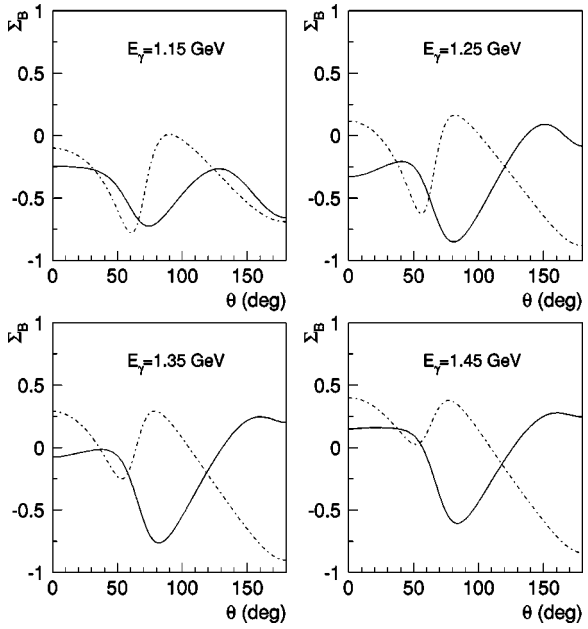

FIG. 8. Beam polarization observable $\check{\Sigma}_B$ at four energy scales. The solid curves denote the full calculations, while the dot-dashed curves denote the $P_{13}(1720)$-absent effects in the full calculations.

In Fig. 8, the full calculations of $\check{\Sigma}_B$ (solid curves) are presented, in which the angular distributions show drastic changes. In comparison with Eq. (19), due to the possible cancellations in the denominator of $\check{\Sigma}_B$, this observable might be sensitive to such effects that are not obvious in $\check{\Sigma}_A$. In fact, we find that the ''defect'' of the Pomeron exchange model can be seen clearly in $\check{\Sigma}_B$ when the exclusive Pomeron exchange is calculated. For the Pomeron exchange model, $\check{\Sigma}_A=+1$ is obtained with a negligible deviation, while for $\check{\Sigma}_B$, large deviations from -1 at middle angles are found. Although the dominant resonance amplitudes can submerge such a ''defect'' efficiently, this observable should be more model dependent than $\check{\Sigma}_A$.

In Ref. [31], the beam polarization is defined as

$$\check{\Sigma}\equiv\vec{\Sigma}\cdot\hat{x}\mathcal{T}=\frac{2\rho^1_{11}+\rho^1_{00}}{2\rho^0_{11}+\rho^0_{00}}, \tag{21}$$

where $2\rho^0_{11}+\rho^0_{00}=1$ represents the normalized cross section function. In this case, the derivation of $\check{\Sigma}$ in experiment requires the integration over angle ϕ. In our previous investigations [16–18], the beam polarization $\check{\Sigma}$ was studied.

Some common features can be derived for the *natural* and *unnatural*-parity exchanges:

(1) For the exclusive *natural* or *unnatural*-parity ex-

[3]From $\check{\Sigma}_A=\pm1$, one cannot directly reach such a conclusion that the exclusive *natural*-or *unnatural*-parity exchange have happened in the reaction, since the asymmetries of the double-flip amplitudes can also lead to the same result.

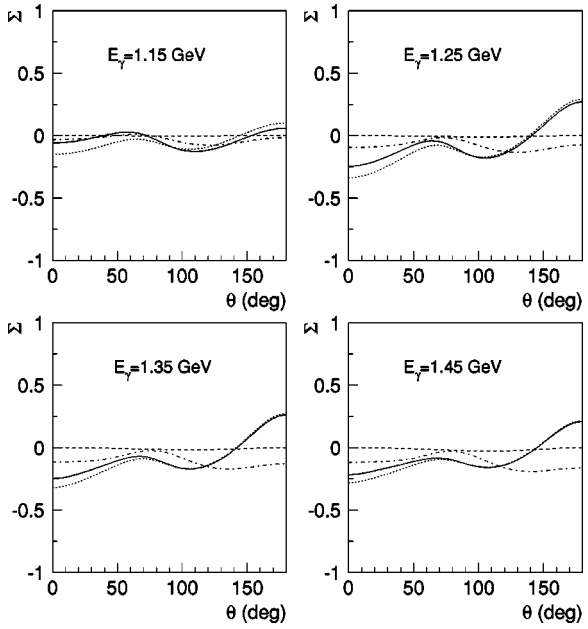

FIG. 9. Beam polarization observable $\check{\Sigma}$ at four energy scales. The notations are the same as Fig. 7.

changes, $\check{\Sigma}$ vanishes due to ρ^1_{11} and $\rho^1_{00}=0$.[4]

(2) With the π^0 plus Pomeron exchanges, this observable almost vanishes since no interferences exist between the real-amplitude π^0 and imaginary-amplitude Pomeron exchanges.

(3) As a direct deduction of the previous two points, large asymmetries can only be produced by other nondiffractive contributions.

In Fig. 9, the calculations of $\check{\Sigma}$ are presented. The solid curves denote the full calculations, while the dashed curves are for the calculations without the *s*- and *u*-channel resonance contributions. We also present the Pomeron-absent results through the dotted curves, of which, however, the changes are not as drastic as in $\check{\Sigma}_A$. The $P_{13}(1720)$-absent effects are also shown by the dot-dashed curves.

[4]Note that the Pomeron, which is rather like an isoscalar photon, will produce a negligible, but nonzero asymmetry in $\check{\Sigma}$.

In comparison with the preliminary study [18], more quantitative results are obtained here through the extensive investigation over the available data.

IV. CONCLUSIONS AND DISCUSSIONS

In this work, we studied three contributing processes in the ω meson photoproduction near threshold. In comparison with the previous approach, here, the introduction of the *t*-channel *natural*-parity Pomeron exchange improves the model predictive power. Although the Pomeron exchange has only small amplitudes near threshold, which does not produce significant effects in the differential cross sections, it has strong interferences with the π^0 exchange terms at forward angles in the beam polarization asymmetries. Taking the advantage of high energy measurement, the Pomeron exchange can be determined. Consequently, the interferences between the Pomeron and π^0 exchanges can be studied with respect to the intermediate-high-energy measurement at small t [14], through which the π^0 exchange can be determined. The reliable constraints found for the *t*-channels highlight the roles played by the resonance excitations. We stress that such a constraint is the prerequisite for the study of resonance excitations in various observables.

Proceeding to the study of the *s*- and *u*-channel resonance excitations in the beam polarization observables, we find that the multiplets of representation $[\mathbf{56},{}^2\mathbf{8},2,2,J]$, i.e., $P_{13}(1720)$ and $F_{15}(1680)$ have large contributions in this reaction. The role played by the $P_{13}(1720)$ is analyzed in the beam polarization asymmetries. This resonance becomes interesting due to its mass position near threshold and relatively larger phase space in the NRCQM. Since its coupling to the ωN has not been known in experiment, the forthcoming data from GRAAL for the beam polarization asymmetries will be able to establish the nature of this resonance in the ωN channel.

ACKNOWLEDGMENTS

The author thanks J.-P. Didelez, M. Guidal, and E. Hourany for useful discussions concerning the GRAAL experiments. Fruitful discussions with Z.-P. Li and B. Saghai are acknowledged. Useful communications with T.-S. H. Lee are acknowledged. This work was supported in part by the ''Bourses de Recherche CNRS-K.C. WONG'' and IPN-Orsay.

[1] N. Isgur and G. Karl, Phys. Lett. **72B**, 109 (1977); Phys. Rev. D **23**, 817 (1981).
[2] R. Koniuk and N. Isgur, Phys. Rev. D **21**, 1868 (1980).
[3] H. Funsten *et al.*, JLab proposal E-91-024.
[4] P. Cole *et al.*, JLab proposal E-94-109.
[5] D. Tedeschi *et al.*, JLab proposals E-97-005 and E-98-109.
[6] F.J. Klein *et al.*, JLab proposal E-99-013.
[7] F.E. Close and Z.-P. Li, Phys. Rev. D **42**, 2194 (1992).
[8] Z.-P. Li and F.E. Close, Phys. Rev. D **42**, 2207 (1992).
[9] S. Capstick, Phys. Rev. D **46**, 2864 (1992).
[10] S. Capstick and W. Roberts, Phys. Rev. D **49**, 4570 (1994).
[11] S. Capstick and W. Roberts, Phys. Rev. D **59**, 014032 (1999).
[12] F.J. Klein, Ph.D. thesis, University of Bonn, Bonn-IR-96-008, 1996; F.J. Klein, πN Newsletter **14**, 141 (1998).
[13] R. Erbe *et al.*, ABBHHM Collaboration, Phys. Rev. **175**, 1669 (1968).
[14] J. Ballam *et al.*, Phys. Rev. D **7**, 3150 (1973).
[15] H.R. Crouch *et al.*, Phys. Rev. **155**, 1468 (1967); Y. Eisenberg *et al.*, Phys. Rev. D **5**, 15 (1972); Y. Eisenberg *et al.*, Phys. Rev. Lett. **22**, 669 (1969); D.P. Barber *et al.*, Z. Phys. C **26**, 343 (1984); W. Struczinski *et al.*, Nucl. Phys. **B108**, 45 (1976).

[16] Q. Zhao, Z.-P. Li, and C. Bennhold, Phys. Lett. B **436**, 42 (1998).
[17] Q. Zhao, Z.-P. Li, and C. Bennhold, Phys. Rev. C **58**, 2393 (1998).
[18] Q. Zhao, Nucl. Phys. **A675**, 217c (2000).
[19] A. Donnachie and P.V. Landshoff, Phys. Lett. B **185**, 403 (1987); Nucl. Phys. **B311**, 509 (1989).
[20] J.-M. Laget and R. Mendez-Galain, Nucl. Phys. **A581**, 397 (1995).
[21] L.P.A. Hackmann, A. Kaidalov, and J.H. Koch, Phys. Lett. B **365**, 411 (1996).
[22] M.A. Pichowsky and T.-S.H. Lee, Phys. Lett. B **379**, 1 (1996); Phys. Rev. D **56**, 1644 (1997).
[23] Q. Zhao, J.-P. Didelez, M. Guidal, and B. Saghai, Nucl. Phys. **A660**, 323 (1999).
[24] Particle Data Group, C. Caso *et al.*, Eur. Phys. J. C **3**, 1 (1998).
[25] A.I. Titov, Y. Oh, and S.N. Yang, Phys. Rev. Lett. **79**, 1634 (1997); A.I. Titov, Y. Oh, S.N. Yang, and T. Morii, Phys. Rev. C **58**, 2429 (1998).
[26] R.G. Moorhouse, Phys. Rev. Lett. **16**, 772 (1966).
[27] Y. Oh, A.I. Titov, and T.-S.H. Lee, nucl-th/0006057.
[28] J.J. Manak *et al.*, Nucl. Phys. **A663&664**, 671c (2000).
[29] B. Friman and M. Soyeur, Nucl. Phys. **A100**, 477 (1996).
[30] K. Schilling, P. Seyboth, and G. Wolf, Nucl. Phys. **B15**, 397 (1970).
[31] M. Pichowsky, Ç. Şavklı, and F. Tabakin, Phys. Rev. C **53**, 593 (1996).